Diurnal Variation of Precipitation over the Tropical Oceans Observed by TRMM/TMI Combined with SSM/I

KEIJI IMAOKA

Earth Observation Research Center, National Space Development Agency of Japan, Tokyo, Japan

ROY W. SPENCER

Global Hydrology and Climate Center, NASA Marshall Space Flight Center, Huntsville, Alabama

(Manuscript received 29 September 1999, in final form 15 May 2000)

ABSTRACT

The Tropical Rainfall Measuring Mission (TRMM) Microwave Imager (TMI) data are used in this study as the first passive microwave information from a precessing orbit to reveal diurnal variations of precipitation over the tropical oceans (30°S–30°N). Data from three Special Sensor Microwave Imagers are combined to help alleviate the aliasing problem caused by the slow diurnal sampling of the TRMM satellite. Annual mean diurnal variations of rainfall in 1998 are presented for 10° latitude bands and six regions. The diurnal variation over all the tropical oceans exhibits an amplitude of about ±14% of the mean, and it peaks near dawn (approximately 0400–0700 LST). By latitude band, diurnal variation is most evident in the deep Tropics, while the ratio of the amplitude over the mean is relatively constant over most latitude bands. Other than in the early morning, there are no evident peaks exceeding the error bars for this analysis. By region, the coastal areas where the ITCZ intersects large continents and around the Maritime Continent are dominant. The morning preference of rainfall prevails almost everywhere in the open ocean where the mean rainfall is heavy, even though the amplitude is small compared to that near the continents.

1. Introduction

The diurnal variation of precipitation over the tropical ocean, where reliable rainfall data have been scarce, still remains an issue in this satellite era. Although the amplitude of the diurnal variation over the ocean is believed to be small compared to that of land, establishing the knowledge of this phenomenon as a consequence of a subtle interaction between dynamical and radiative processes is important to complete our understanding of convective activity. From the point of view of satellite remote sensing, this knowledge is indispensable to interpret temporally intermittent measurements from polar orbiting satellites. To construct long-term satellite records, the correction for the diurnal cycle is one of the serious problems to solve. Even for a series of identical sensors, since the equatorial crossing time differs from satellite to satellite, and usually drifts year by year, we need to remove this diurnal drift or offset that can falsely suggest a long-term trend.

Numerous authors have studied the diurnal variation of rainfall over the tropical oceans using satellite measurements. Because of the frequent observing capability, many investigators used infrared data from geostationary meteorological satellites, even though they cannot be considered as direct information on rainfall. Augustine (1984), Albright et al. (1985), Meisner and Arkin (1987), and Shin et al. (1990) used fractional coverage by cold cloud as an indication of deep convection. Hendon and Woodberry (1993), Murakami (1983), and Nitta and Sekine (1994) used indices of deep convective activity, although their definitions of the index were somewhat different from each other. Fu et al. (1990) partitioned rainfall into two categories (deep convective and cirrus anvil) by combining infrared and visible information. They found that the frequency of the cirrus anvil component exhibits a peak in the midafternoon, while the deep convective cloud portion peaks 9–12 h earlier. Janowiak et al. (1994) found that the time of maximum occurrence of cold cloud varies with the temperature threshold employed. Coldest cloud-top temperatures (<215 K) were found to occur much earlier in the day than those of warmer cloud tops and peaked between 0300 and 0600 local solar time (LST). Mapes and Houze (1993) discussed the different infrared temperature thresholds used by many investigators. They also discussed the cluster-size dependence of the diurnal cycle in very cold cloudiness.

Corresponding author address: Keiji Imaoka, Earth Observation Research Center, National Space Development Agency of Japan, 1-9-9 Roppongi, Minatu-ku, Tokyo 106-0032, Japan.
E-mail: imaoka@eorc.nasda.go.jp

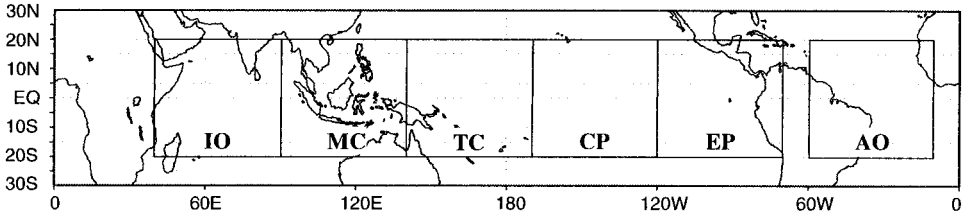

FIG. 1. Definition of the regions. Solid lines delineate the six geographical regions: Indian Ocean (IO), Maritime Continent (MC), TOGA COARE domain (TC), central Pacific (CP), east Pacific (EP), and Atlantic Ocean (AO). All the statistics were computed only over the ocean.

Passive microwave techniques are known to offer a more direct signal from the rain layer. Since all the microwave sensors have been on board sun-synchronous platforms, those provide only two samples per day. Kidder and Vonder Haar (1977) analyzed the *Nimbus-5* microwave brightness temperatures (Tb's). In Sharma et al. (1991), investigation of the diurnal variation using Defense Meteorological Satellite Program (DMSP) Special Sensor Microwave Imager (SSM/I) data, the average ratio of morning to afternoon rainfall was about 1.2 by averaging the data over a large area ($\pm 50°$ latitude). Chang et al. (1995) also examined SSM/I-derived rainfall. The morning rainfall estimates were larger than those of evening by approximately 20% over the ocean between $\pm 50°$ latitude. The differences were most significant along the intertropical convergence zone (ITCZ) region.

Although some of the infrared results seem to be in conflict with each other and the phenomenon seems to be different from region to region, most of the results including all the microwave observations show a nocturnal or early morning rainfall maximum over the ocean.

Simulation studies using general circulation models such as Randall et al. (1991) also show a maximum of precipitation in early morning over the oceans far from land. They concluded that daytime stabilization of the cloud layer due to solar heating of upper-tropospheric clouds tends to suppress convection during the afternoon. Liu and Moncrieff (1998) also obtained a significant diurnal cycle of precipitation with a nocturnal and early morning peak by using an idealized two-dimensional cloud-resolving numerical model. Gray and Jacobson (1977) hypothesized that mesoscale pressure gradients created by differences of the radiative heating/cooling between cloudy and adjacent clear regions cause the morning-maximum diurnal cycle of precipitation over the ocean.

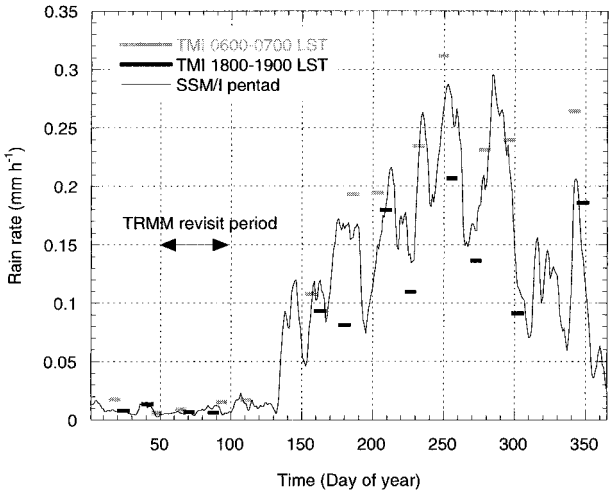

FIG. 2. Temporal variation of SSM/I rain rates (pentad-running mean) in 10°–20°N latitude band with TMI rain rates in two local time bins. TMI rain rates are averaged over the period of one sample (indicated by the length of line).

The Tropical Rainfall Measuring Mission (TRMM) satellite was launched into a non-sun-synchronous orbit with an inclination angle of 37° and the altitude of 350 km. The instrument package consists of the precipitation radar (PR), the TRMM Microwave Imager (TMI), the visible-infrared scanner (VIRS), the lightning imaging sensor, and the Clouds and the Earth's Radiant Energy System. Because of the characteristics of the orbit, the equatorial crossing time gradually varies, providing information on the diurnal variation of geophysical parameters. Since TMI is the first passive microwave radiometer put into a non-sun-synchronous orbit, this is the first opportunity to investigate complete diurnal variation (not a two-point measurement per day in time by a polar orbiting instrument like SSM/I) of precipitation with more direct information on the rain layer than infrared observations. The objective of this paper is, by utilizing the advantages mentioned above, to provide a 1998 annual mean diurnal variation of precipitation and its latitudinal/regional characteristics over the tropical oceans using the TMI, combined with polar orbiting microwave information (SSM/I).

2. Data and methodology

Daily binary data files of geophysical parameters produced by Remote Sensing Systems were mainly used in this study. They consist of 0.25° by 0.25° gridded maps including observation time, sea surface temperature (only for TMI), wind speed, total water vapor, cloud liquid water, and precipitation rate for ascending and descending orbits separately. The technique for es-

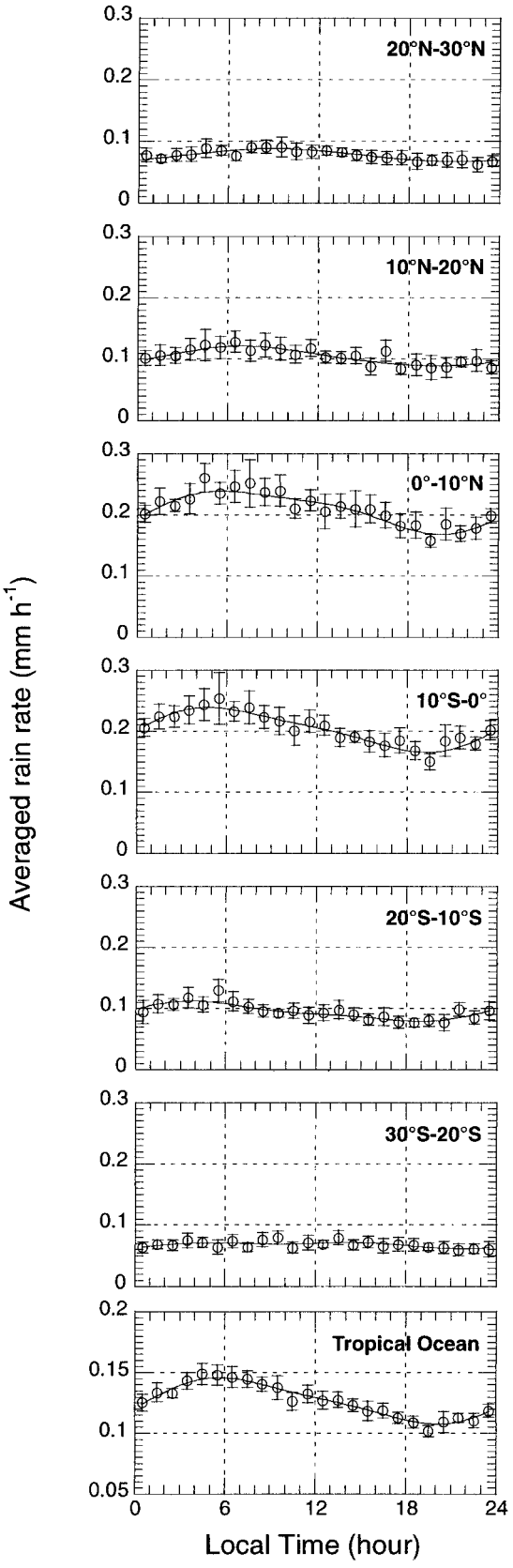

FIG. 3. Diurnal variation in six latitude bands over the tropical oceans. The error bars indicate 95% statistical confidence.

timating instantaneous rain rates from SSM/I data was described in detail by Wentz and Spencer (1998). In short, it is a physically based emission algorithm unified with the all-weather ocean retrieval of the other geophysical parameters. Rain rates are available over the ocean up to about 25 mm h^{-1}. A beamfilling correction is made, based on the ratio of the retrieved liquid water absorption coefficients at 37 and 19 GHz. The same algorithm is applied to TMI and SSM/I, except for small differences of channel frequency and earth incidence angle. The current algorithm does not utilize the newly added 10-GHz frequency of TMI, which is more transparent to the rain layer and has a more linear relationship between Tb and the rain rate. This reduces our dataset's sensitivity to heavier rain rates. To obtain an annual mean of the diurnal precipitation variation over the tropical oceans, we used TMI rain rates from 1998 over 30°S–30°N latitudes. Three SSM/Is flying on the DMSP *F-11*, *F-13*, and *F-14* satellites in 1998 were also used. The mean of SSM/I equatorial crossing times in 1998 were 0719, 0551, and 0841 LST for *F-11*, *F-13*, and *F-14*, respectively. The largest drift of equatorial crossing time was less than 15 min per year for *F-11*, and we considered this as negligible.

We first intercalibrated the rain rates of TMI with those from the three different SSM/Is. Since the equatorial crossing time is different for the different SSM/Is, we compared each SSM/I with TMI in 0.25° grids within ±6-min time difference. Average ratios of 0.64, 0.62, and 0.60 were found for *F-11*, *F-13*, and *F-14* over TMI, respectively. One of the possible reasons of this discrepancy is related to the difference of spatial resolution. Although this discrepancy is not small, we simply employed the value of 0.62 as the conversion coefficient from TMI to SSM/I at this time.

In order to obtain statistically stable results, we only computed the annual mean diurnal variation over the tropical oceans. TMI data were binned by 1-h local time and stratified two different ways: 10° latitude bands and six geographical regions (±20° latitude by 45° longitude, shown in Fig. 1). SSM/I rain rates were used combined with TMI rain rates, as described later. Independently, SSM/I data were also stratified by the same latitude band/region for morning and evening orbits separately. During the TRMM precessing period (approximately 48 days), we have only two opportunities to observe a given area in each local time bin using both ascending and descending orbit data. This means only about 15 samples (at maximum) of the diurnal cycle are available during a year. We considered these as independent samples in this analysis. Temporal rainfall fluctuations (longer than a day, if any) add noise to our estimates of the diurnal cycle. This is particularly critical with a restricted number of samples. Variations in the timescale shorter than the TRMM revisit period, which cannot be canceled with TRMM data alone, introduce aliasing. To help alleviate the effects of these variations superimposed on the diurnal signal, we used

TABLE 1. Amplitude and phase of the first harmonic with hourly averages of rain rate in (a) six latitude bands and (b) six geographical regions. The attached uncertainty is standard error. Values are not shown if the error exceeds them.

(a) Latitude band	Average (mm h^{-1})	Amplitude (mm h^{-1})	Amplitude/Average (%)	Phase (h)
20°–30°N	0.078	0.010 ± 0.005	12.8	9.0 ± 1.8
10°–20°N	0.105	0.016 ± 0.008	15.2	7.3 ± 1.6
0°–10°N	0.211	0.033 ± 0.009	15.6	7.5 ± 1.0
10°S–0°	0.205	0.034 ± 0.009	16.6	6.2 ± 0.9
20°–10°S	0.096	0.015 ± 0.006	15.6	4.9 ± 1.5
30°–20°S	0.068	—	—	—
Tropics	0.127	0.018 ± 0.003	14.2	6.9 ± 0.7
(b) Region	Average (mm h^{-1})	Amplitude (mm h^{-1})	Amplitude/Average (%)	Phase (h)
Indian Ocean	0.158	0.017 ± 0.009	10.8	6.0 ± 2.1
Maritime Continent	0.228	0.051 ± 0.011	22.4	7.4 ± 0.9
TOGA COARE	0.171	0.031 ± 0.010	18.1	5.5 ± 1.3
Central Pacific	0.160	0.021 ± 0.009	13.1	5.4 ± 1.6
East Pacific	0.142	0.026 ± 0.010	18.3	7.3 ± 1.5
Atlantic Ocean	0.103	0.014 ± 0.009	13.6	7.0 ± 2.3

the SSM/I rain rates when stratifying TMI data. Because of incomplete daily coverage by SSM/I (even if three sensors are used), we used pentad-running averaged grid points (averaged over 5 days, morning and evening, and three SSM/Is) of SSM/I rainfall instead of daily grid points. For given local time bin and band/region, the annual mean of rain rates was computed in the following manner. Daily gridpoint rainfall differences between TMI instantaneous (R_{TMI}) and SSM/I pentad-running mean (R_{SSMI}) were averaged over the period of one sample, then further averaged over a prescribed area by

$$\overline{D}_R(s) = \frac{1}{N_T N_d} \sum_{i=1}^{N_T} \sum_{d=1}^{N_d} [R_{\mathrm{TMI}}(i, d) - R_{\mathrm{SSMI}}(i, d)], \quad (1)$$

where N_d is the number of days when TMI observed the grid point i during the period of sample s, and N_T is the total number of grids in the area. The value of N_d depends on latitude, ranging from 1 or 2 near the equator, to 1 to 3 near 30° latitude. Although there are very small areas where $N_d = 0$, particularly near the equator, we did not include those areas in the calculation. The annual mean of rainfall differences was calculated by

$$\overline{D}_R = \frac{1}{N_s} \sum_{s=1}^{N_s} \overline{D}_R(s), \quad (2)$$

where N_s is a number of samples in a year. Error bars of 95% confidence were computed with the assumption of normal distribution of samples. The annual mean rain rate at each local time bin was

$$\overline{R} = \overline{D}_R + \overline{R}_{\mathrm{SSMI}}, \quad (3)$$

where $\overline{R}_{\mathrm{SSMI}}$ is an annual mean of R_{SSMI} that was used in Eq. (1). To show the relationship between TMI sampling and temporal rainfall variability, a pentad-running averaged time series of SSM/I rainfall in 10°–20°N latitude band is shown as an example in Fig. 2, with TMI rain rates in two local time bins. Although the statistical

TABLE 2. SSM/I morning and evening rain rates in (a) six latitude bands and (b) six geographical regions.

(a) Latitude	AM (mm h^{-1})	PM (mm h^{-1})	Average (mm h^{-1})	(AM–PM)/2 (mm h^{-1})	(AM–PM)/2/Average (%)
20°–30°N	0.089	0.071	0.080	0.009	11.3
10°–20°N	0.124	0.088	0.106	0.018	17.0
0°–10°N	0.247	0.165	0.206	0.041	19.9
10°S–0°	0.240	0.156	0.198	0.042	21.3
20°–10°S	0.108	0.079	0.094	0.015	15.7
30°–20°S	0.081	0.072	0.076	0.005	6.1
Tropics	0.152	0.107	0.130	0.022	17.3
(b) Region	AM (mm h^{-1})	PM (mm h^{-1})	Average (mm h^{-1})	(AM–PM)/2 (mm h^{-1})	(AM–PM)/2/Average (%)
Indian Ocean	0.173	0.126	0.150	0.023	15.4
Maritime Continent	0.288	0.163	0.225	0.062	27.7
TOGA COARE	0.200	0.139	0.170	0.030	17.9
Central Pacific	0.179	0.139	0.159	0.020	12.5
East Pacific	0.174	0.114	0.144	0.030	20.6
Atlantic Ocean	0.116	0.082	0.099	0.017	17.3

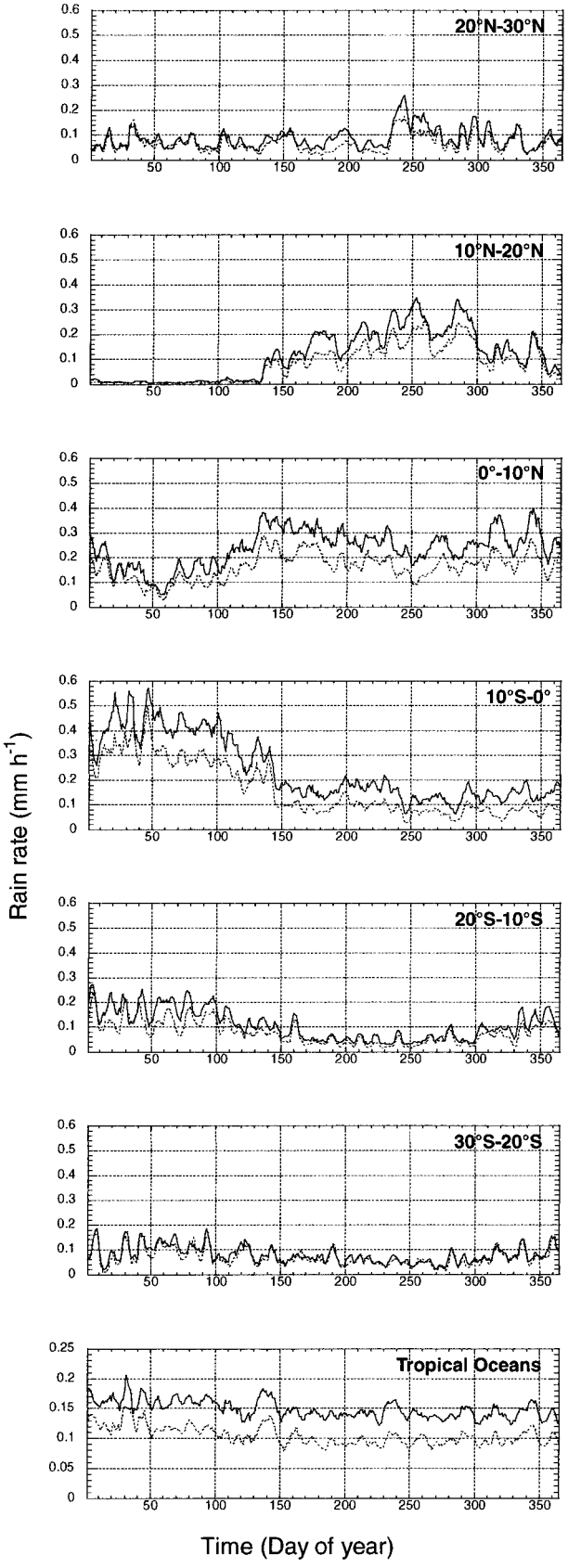

treatment in this analysis is not perfect (e.g., we ignore the time correlation of rainfall), we believe that this will not change our results significantly because of the large averaging area and the long averaging time. Bell and Reid (1993) discussed a more thorough statistical treatment of this kind of analysis.

To briefly examine the validity of computed diurnal variation of precipitation, we also used two different TRMM products: TMI rainfall (2A12) and combined TMI/PR rainfall (2B31). Both products are distributed by the Goddard Space Flight Center (GSFC) Earth Sciences Distributed Active Archive Center (DAAC) as TRMM Gridded Orbital Data. Data were simply stratified over all the tropical oceans by 1-h local time bins.

3. Results and discussion

a. Diurnal variation in the latitude bands

The annual means of diurnal variations in six latitude bands over the tropical oceans are shown in Fig. 3. TMI provided us this sort of full and continuous diurnal variation for the first time, even though they are annual means over a large area. The error bar does not represent the absolute accuracy of annual mean rainfall at each local time but indicates the significance of relative differences among local time bins. A harmonic analysis was performed on those annual means. The amplitude and phase of the first harmonic are summarized in Table 1a. Although the second harmonic component is included in the curve fit, the values are not shown due to their insufficient statistical significance in this analysis. A diurnal variation in precipitation is clearly seen in the deep Tropics. Within 10°S–10°N, the peak-to-peak difference is about 0.07 mm h^{-1}, which corresponds to about ±16% of the mean. The peak occurs near dawn (0300–0700 LST) and the minimum in the evening (1800–2200 LST). In higher-latitude bands, except in 30°–20°S, weaker diurnal variations are significant, yet their ratios to the mean are relatively comparable to that of the deep Tropics. Generally speaking, no peaks are seen other than those near dawn. Although the second harmonic component plays some role in fitting the data, its contribution to the amplitude is less significant than that of the first harmonic. Consequently, the diurnal variation over all the tropical oceans shows a smooth shape having a maximum at about 0400–0700 LST and minimum at 1900–2100 LST. The peak-to-peak amplitude is about ±14% of the mean. The amplitude of the second harmonic is less than 30% of that of the first harmonic, having two peaks at around 0400 and 1600 LST (not shown).

←

FIG. 4. Pentad-averaged time series of SSM/I morning (solid) and evening (dotted) rain rates in six latitude bands and all the tropical oceans. Note the different scale of rain rates for the entire tropical oceans.

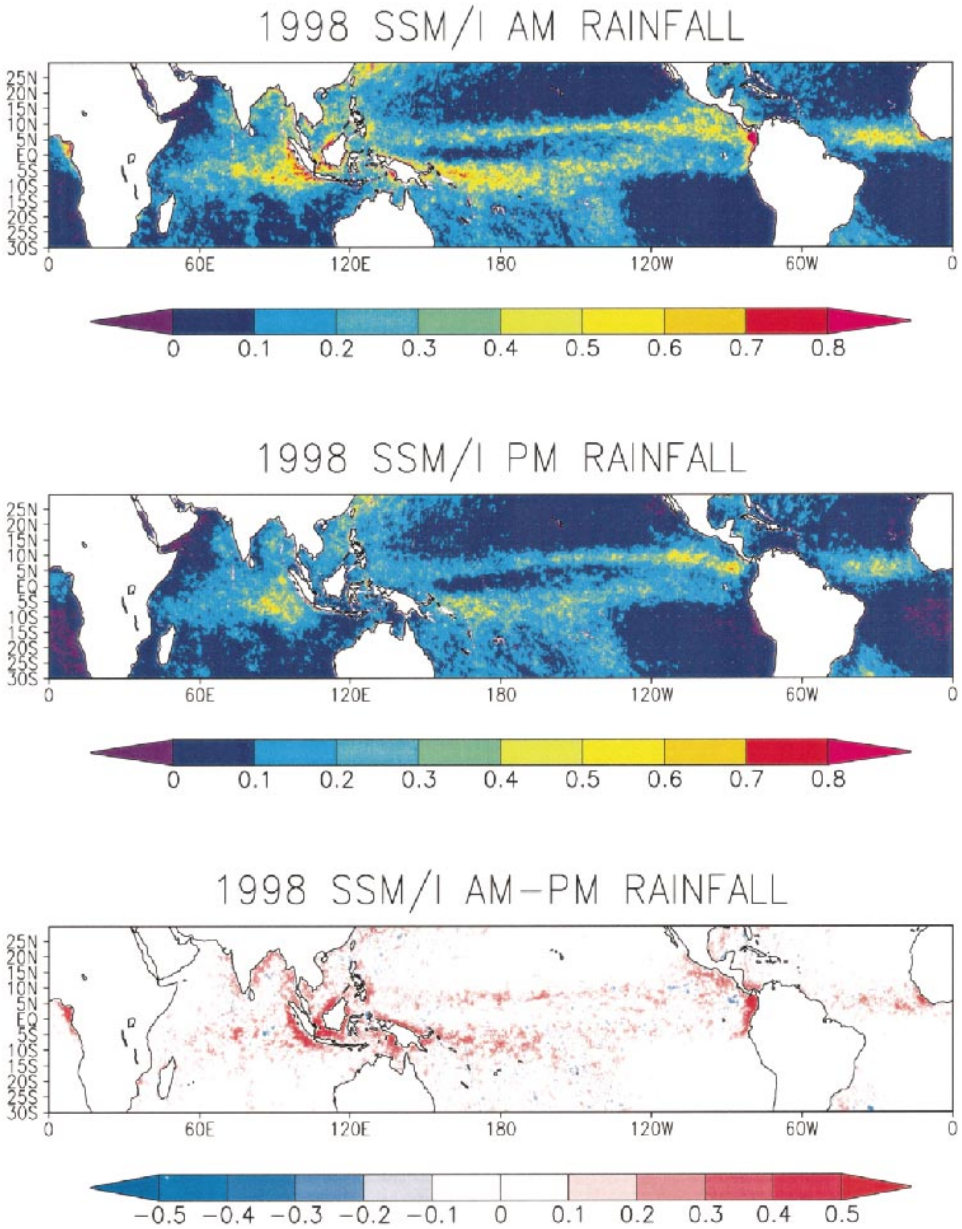

FIG. 5. SSM/I annual mean rainfall rates for the morning (top) and the evening (middle) measurement. Differences (morning minus evening) are also shown in the bottom figure. Units for all are mm h^{-1}.

The pentad-averaged time series of SSM/I rainfall by latitude band is shown in Fig. 4. Since no evident subpeaks are seen in Fig. 3 and the local solar time of SSM/I almost coincides with the maximum and minimum of rainfall, the variation of differences between morning and evening rainfall in Fig. 4 may be considered as an index of the diurnal amplitude of rainfall. Morning rainfall is larger than evening rainfall in most latitude bands throughout the year. In all the tropical oceans, the diurnal cycle accounts for a large part of the rainfall variance year-round. The amplitude of the diurnal variation seems to correlate with rainfall rate, and there is some evidence of a seasonal variation of diurnal amplitude. In the 20°–30°N band, the diurnal amplitude during winter season (in the Northern Hemisphere) seems to be smaller than that of summer season, in spite of nearly the same rainfall rate. Since the daily passage of the Sun must control the diurnal variation of rainfall, it is reasonable to expect a weaker diurnal signal during the winter season, regardless of its precise mechanism. The annual average of morning and evening SSM/I rainfall is summarized in Table 2a by the latitude band. The ratio of, as well as the difference between, morning and evening rainfall tends to decrease as latitude increases,

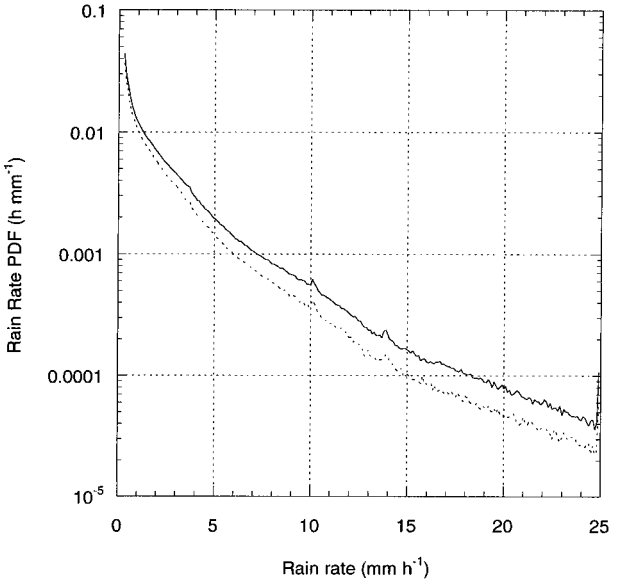

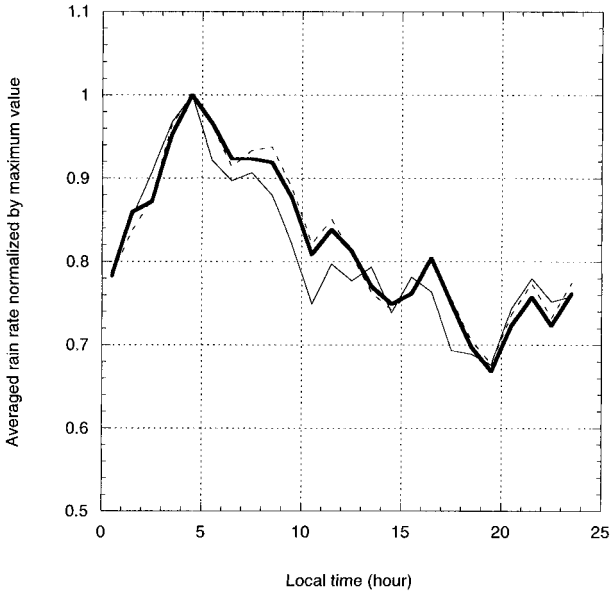

FIG. 7. Comparison of diurnal rainfall variations derived from three different TRMM products: TMI rainfall processed by Remote Sensing Systems (thick solid), 2A12 TMI rainfall (dotted), and 2B31 TMI/PR combined rainfall (solid). Rain rates are normalized by their maximum values.

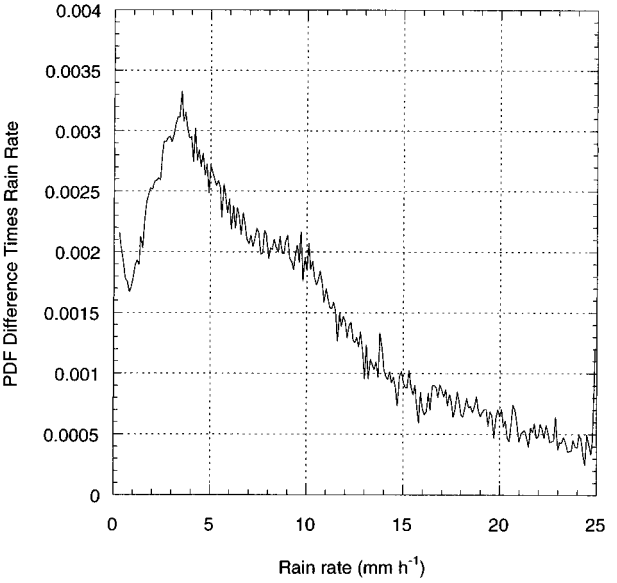

FIG. 6. Contribution of the footprint-averaged SSM/I rain rates to the morning − evening difference of rainfall. Only the rain rates between 0.2 and 25.0 mm h^{-1} are shown in the figures. (a) The PDF for rain rate. The solid and dotted curve show morning and evening PDF, respectively. (b) Morning − evening differences of PDF multiplied by rain rate.

as is seen in the combined result of TMI and SSM/I. The ratio for all the tropical oceans is about 1.42, which is close to the value of 1.44 reported by Petty and Katsaros (1992), when their ratio is averaged over the tropical oceans, summer and winter (their ratio is not based on rain rates but on the number of rainy grids). The percentages in Table 2 differ somewhat from those in Table 1. Our intercalibration coefficient is only the ratio of means and may not be enough to represent nonlinearity and biases. This, as well as slight differences between actual local time of rainfall maximum/minimum and SSM/I observing local time, probably accounts for the differences in percentages.

b. Regional characteristics

The results of the harmonic analysis for each region are shown in Table 1b. The most apparent diurnal cycle is seen around the Maritime Continent (MC; 90°–40°E). The peak-to-peak amplitude almost reaches half of the mean. The diurnal variation is also prominent in the Tropical Ocean and Global Atmosphere Coupled Ocean–Atmosphere Response Experiment (TOGA COARE) region (TC; 140°E–170°W). The tendency of a morning rainfall maximum is also observed in almost all the other regions, although their amplitude is weak compared to the error of this analysis. The SSM/I statistics (Table 2b) also show the morning preference of rainfall in all the regions.

The regional features are more clearly seen in the maps of the annual mean SSM/I rainfall for morning and evening (Fig. 5). The most evident differences are observed in coastal areas, particularly in the MC region and the coasts where the ITCZ intersects South America and Africa. These are consistent with previous infrared studies, while none of previous microwave results showed this due to the exclusion of near-land pixels in

order to avoid the contamination of land emission into a large-size grid (e.g., 5° × 5°). The TC region also shows a clear difference. Thus, those regions almost dominate the diurnal variation over the deep Tropics seen in Fig. 3. While we do not have any direct evidence in this analysis, there are two possible explanations of this regional characteristic. One is the interaction between land and sea breeze with the synoptic wind field (Houze et al. 1981; Oki and Mushiake 1994), and the other is the hypothesis of Silva Dias et al. (1987) that large continents modulate the diurnal cycle of convection over the neighboring oceanic regions.

As seen in Fig. 5, the tendency of a morning maximum is still significant in the open ocean far from land, particularly along the ITCZ. Daytime stabilization of the cloud layer due to solar heating of the upper-tropospheric cloud is one of the possible mechanisms of morning preference of rain (Randall et al. 1991). As discussed by Mapes and Houze (1993), however, this does not necessarily explain the cluster-size dependence of the diurnal variation. In addition, as also discussed by them, it is not clear if upper-tropospheric stabilization could control the strong low-level convergence particularly along the ITCZ. The evening preference of rain is seen in only a few isolated regions such as the ITCZ in the northeastern Pacific and near the central area of the Indian Ocean.

The morning preference of rain is consistent with many previous infrared studies in which the very cold cloud-top temperature (~210 K) threshold was adopted for calculating fractional coverage, or cirrus anvil was excluded by combining visible information (e.g., Janowiak et al. 1994; Fu et al. 1990; Mapes and Houze 1993). It has been discussed that the afternoon maximum of rainfall detected by fractional coverage methods with warmer infrared temperature threshold (~235 K) is probably related to cirrus anvils, which is a lagged response to active deep convection. Deep convective indices seem to represent rainfall better than fractional coverage, regardless of their threshold of cloud-top temperatures. The present analysis further supports the position that, at least as the average over all the tropical oceans, there is no afternoon maximum in tropical oceanic rainfall.

c. Probability density functions of SSM/I rain rates

The probability density function (PDF) for the SSM/I footprint-averaged rain rates over all the tropical oceans is illustrated in Fig. 6a. The solid and dotted lines show morning and evening rainfall, respectively. The morning-to-evening ratio (difference in log-scale axis) is larger at heavier rainfall. Figure 6b shows the morning − evening difference of PDF multiplied by the rain rate. This curve indicates the contribution of the various footprint-averaged rain rates to the morning − evening rainfall difference. The area under the curve equals the averaged-rainfall difference between morning and evening. One-half of the rainfall difference occurs at footprint-averaged rain rates above 8.5 mm h^{-1}, while it corresponds to only approximately 10% of the total number of rainfall observations. These suggest that heavier rainfall events tend to occur in the morning and contribute considerably to the morning − evening difference of rainfall, despite their small probability of occurrence. Mapes and Houze (1993) concluded that the diurnal cycle of cold cloudiness is primarily a sun-synchronous process within large and giant clusters, not a modulation of populations of isolated convective clouds. They found that numerous clusters are observed during early morning and fewer in the evening hours. Therefore, the morning maximum of rainfall is probably dominated by matured clusters with deep convective rain, possibly accompanied by a considerable amount of stratiform type of rain. Since the SSM/I as well as TMI data possibly miss heavier rainfall due to signal saturation and/or the beamfilling problem, we need to further investigate this by analyzing the PR rainfall. The PR will also provide information on the contributions by different types of rainfall to the diurnal variation (convective, stratiform, warm rain, etc.). The sensitivity of the TMI algorithm to heavier rain rates would be improved by including the 10-GHz channels. It should be also noted that the footprint-averaged rain rate cannot be directly compared to small-scale rain rate such as that measured by the rain gauge (Wentz and Spencer 1998).

d. TRMM and polar-orbiting satellite

Combining the data of TMI and SSM/I to help alleviate the aliasing problem was effective in reducing noise at each local time bin and in obtaining a reliable shape of diurnal variation. In terms of annual mean rainfall as the integral of diurnal curve, however, the combination method did not improve the accuracy very much. As for separate latitude bands, the largest difference of annual mean rainfall between the combined result and the TMI-only (simple stratification of TMI data into local time bins) result is only 5% in the 10°–20°N latitude band. As the averaging area becomes smaller or averaging period becomes shorter, the error may increase and therefore the combination becomes more important.

As noted before, the equatorial crossing time of SSM/I happens to coincide with the maximum and minimum of diurnal rainfall variation. Thus, due to the smooth diurnal change of rainfall as seen in Fig. 3, the SSM/I annual mean rainfall over the tropical oceans is considered as a reasonable estimate of true value. Since the diurnal variation on smaller spatial scales is more complicated, however, the SSM/I estimate suffers from the aliasing problem.

e. Comparison with other products

As noted by Wentz and Spencer (1998), there still remains the problem of absolutely calibrating their rain

algorithm. Thus, the absolute amplitude of the diurnal variation listed in Tables 1 and 2 needs to be further validated. We believe, however, that the relative ratio of the amplitude to the mean and phase are reasonable. Comparison with other TRMM products supports the present results. Figure 7 shows the annual means of diurnal variation over all the tropical oceans derived by three different rainfall products, TMI processed by Remote Sensing Systems, TMI rainfall (2A12), and TMI/PR combined (2B31). Rain rates are normalized by their maximum values. Since these are derived by simple stratification of each rain rate (not the combined results with SSM/I), the diurnal variations somewhat differ from that of Fig. 3. As mentioned in section 2, the rainfall algorithm of Remote Sensing Systems is an emission-based method, while that of TMI rainfall (2A12) utilizes not only emission but also scattering. The TMI/PR combined (2B31) product should reflect the characteristics of PR. In spite of possible differences among these products in terms of algorithm and measurement principle, the diurnal patterns are very similar.

4. Summary

TMI, the first passive microwave imager on board a non-sun-synchronous satellite provides direct information on the diurnal variation of tropical rainfall. We have examined the 1998 annual mean diurnal variation of precipitation over the tropical oceans using the TMI combined with SSM/I measurements. The SSM/I data at fixed local solar times were useful to help alleviate the aliasing problem caused by the slow diurnal sampling of TRMM. The diurnal variation averaged over all the tropical oceans exhibits an amplitude of about $\pm 14\%$ of the mean, and it peaks at near dawn (approximately 0400–0700 LST). The diurnal variation is most evident in the deep Tropics, while the ratio of the amplitude over the mean is relatively constant over most latitude bands. By region, coastal areas where the ITCZ intersects the large continents and the Maritime Continent exhibit strong diurnal variation. This is probably explained by the low-level convergence between land breeze and large-scale wind systems. The morning preference of rainfall exists almost everywhere in the open ocean where the mean rainfall is heavy, even though the amplitude is small compared to that near the continents. It is suggested that the midafternoon maximum of rainfall sometimes inferred from infrared observations with a warmer threshold of cold cloud-top temperature (e.g., 235 K) for calculating fractional coverage does not represent the rainfall maximum, but is probably due to residual anvil cirrus effect lagging the peak in deep convection.

Further study using other TRMM sensors should be performed to investigate possible differences among different methods of rainfall retrieval. More detailed analysis of the PR would supplement or confirm the TMI result as an independent measurement of precipitation information. The PR would also provide the diurnal variation of rain type as well as storm height. Describing the difference between TMI and VIRS would be invaluable to understand the relationship of the infrared measurement from geostationary orbit to diurnal variations in rainfall. An analysis of diurnal variation in terms of smaller spatial scale and seasonal change could be investigated by using multi year TRMM data.

Acknowledgments. TMI and SSM/I binary data files were obtained via anonymous ftp from Remote Sensing Systems. The authors wish to thank the GSFC DAAC for producing and distributing the TRMM Gridded Orbital Data, and the TRMM Science Data and Information System at the GSFC, for providing the original data from which this product originates. Goddard's contribution to these activities was sponsored by NASA's Earth Science Enterprise. The subject of this research was first suggested by Christian Kummerow (NASA GSFC). This work was carried out during the visit of the first author to the Global Hydrology and Climate Center, NASA Marshall Space Flight Center. The first author thanks Elena Lobl for providing overall support for the visit, and to colleagues in the MSFC Microwave Measurements Group for informative discussions.

REFERENCES

Albright, M. D., E. E. Recker, R. J. Reed, and R. Dang, 1985: The diurnal variation of deep convection and inferred precipitation in the central tropical Pacific during January–February 1979. *Mon Wea. Rev.,* **113,** 1663–1680.

Augustine, J. A., 1984: The diurnal variation of large-scale inferred rainfall over the tropical Pacific Ocean during August 1979. *Mon. Wea. Rev.,* **112,** 1745–1751.

Bell, T. L., and N. Reid, 1993: Detecting the diurnal cycle of rainfall using satellite observations. *J. Appl. Meteor.,* **32,** 311–322.

Chang, A. T. C., L. S. Chiu, and G. Yang, 1995: Diurnal cycle of oceanic precipitation from SSM/I data. *Mon. Wea. Rev.,* **123,** 3371–3380.

Fu, R., A. D. Del Genio, and W. B. Rossow, 1990: Behavior of deep convective clouds in the tropical Pacific from ISCCP radiances. *J. Climate,* **3,** 1129–1152.

Gray, W. M., and R. W. Jacobson Jr., 1977: Diurnal variation of deep cumulus convection. *Mon. Wea. Rev.,* **105,** 1171–1188.

Hendon, H. H., and K. Woodberry, 1993: The diurnal cycle of tropical convection. *J. Geophys. Res.,* **98,** 16 623–16 637.

Houze, R. A., Jr., S. G. Geotis, F. D. Marks Jr., and A. K. West, 1981: Winter monsoon convection in the vicinity of north Borneo. Part I: Structure and time variation of the clouds and precipitation. *Mon. Wea. Rev.,* **109,** 1595–1614.

Janowiak, J. E., P. A. Arkin, and M. Morrissey, 1994: An examination of the diurnal cycle in oceanic tropical rainfall using satellite and in situ data. *Mon. Wea. Rev.,* **122,** 2296–2311.

Kidder, S. Q., and T. H. Vonder Haar, 1977: Seasonal oceanic precipitation frequencies from *Nimbus-5* microwave data. *J. Geophys. Res.,* **82,** 2083–2086.

Liu, C., and M. W. Moncrieff, 1998: A numerical study of the diurnal cycle of tropical oceanic convection. *J. Atmos. Sci.,* **55,** 2329–2344.

Mapes, B. E., and R. A. Houze Jr., 1993: Cloud clusters and superclusters over the oceanic warm pool. *Mon. Wea. Rev.,* **121,** 1398–1415.

Meisner, B., and P. Arkin, 1987: Spatial and annual variations in the

diurnal cycle of large-scale tropical convective cloudiness and precipitation. *Mon. Wea. Rev.*, **115,** 2009–2032.

Murakami, M., 1983: Analysis of the deep convective activity over the western Pacific and Southeast Asia. Part I: Diurnal cycle. *J. Meteor. Soc. Japan.*, **61,** 60–75.

Nitta, T., and S. Sekine, 1994: Diurnal variation of convective activity over the tropical western Pacific. *J. Meteor. Soc. Japan,* **72,** 627–640.

Oki, T., and K. Mushiake, 1994: Seasonal change of the diurnal cycle of precipitation over Japan and Malaysia. *J. Appl. Meteor.*, **33,** 1445–1463.

Petty, G. W., and K. B. Katsaros, 1992: Morning-evening differences in global and regional oceanic precipitation as observed by the SSM/I. Preprints, *Sixth Conf. on Satellite Meteorology and Oceanography,* Atlanta, GA, Amer. Meteor. Soc., 282–285.

Randall, D. A., Harshvardhan, and D. A. Dazlich, 1991: Diurnal variability of the hydrologic cycle in a general circulation model. *J. Atmos. Sci.*, **48,** 40–62.

Sharma, A., A. Chang, and T. Wilheit, 1991: Estimation of the diurnal cycle of oceanic precipitation from SSM/I data. *Mon. Wea. Rev.*, **119,** 2168–2175.

Shin, K.-S., G. R. North, Y.-S. Ahn, and P. A. Arkin, 1990: Time scales and variability of area-averaged tropical oceanic rainfall. *Mon. Wea. Rev.*, **118,** 1507–1516.

Silva Dias, P. L., J. P. Bonatti, and V. E. Kousky, 1987: Diurnally forced tropical tropospheric circulation over South America. *Mon. Wea. Rev.*, **115,** 1465–1478.

Wentz, J. F., and R. W. Spencer, 1998: SSM/I rain retrievals within a unified all-weather ocean algorithm. *J. Atmos. Sci.,* **55,** 1613–1627.